Patterns and Drivers of Dissolved Gas Concentrations and Fluxes Along a Low Gradient Stream

Authors: Alice M. Carter[1,2], Amanda G. DelVecchia[1], and Emily S. Bernhardt[1]

[1]Duke University, Durham, NC.

[2]Flathead Lake Biological Station, University of Montana, Missoula, MT.

Corresponding author:

Alice M Carter (alice.m.carter@flbs.umt.edu) ORCID: 0000-0002-7225-7249

Amanda G DelVecchia ORCID: 0000-0003-4252-5991

Emily S Bernhardt ORCID: 0000-0003-3031-621X

Key Points (140 characters or less):

- Patterns in carbon dioxide are almost entirely accounted for by instream metabolism except during a storm event.
- Methane is highly variable in space and scales with aerobic respiration.
- The stream shifts from a source of nitrous oxide to a sink during peak autumn respiration, likely due to nitrogen limitation.

Keywords (up to six):

Greenhouse gas, Streams, Carbon, Metabolism

Index Terms:

Primary: Ecosystems, structure, and dynamics

1. Trace gases
2. Carbon cycling
3. Oxidation reduction reactions

Cover letter (optional): *The data for this manuscript were collected over three seasons, autumn, winter, and spring ending in March 2020. The original intent was to continue sampling through the summer, but that was not possible given research restrictions associated with the COVID-19 pandemic shutdown at Duke University. We hope that editors and reviewers will note this in the assessment of the overall study.*

Suggested editor(s):

1. Marguerite Xenopoulos
2. Deborah Huntzinger

Suggested reviewers:

1. Jackie Webb, Deakin University
2. Nathan Barros, Radboud University
3. Shaoda Liu, Yale
4. Kimberly van Meter, Penn State
5. Adam Wymore, UNH

Abstract

Freshwater ecosystems are globally significant sources of greenhouse gases (GHG) to the atmosphere. Generally, we assume that in-situ production of GHG in streams is limited by turbulent reaeration and high dissolved oxygen concentrations, so stream GHG flux is highest in headwater streams that are connected to their watersheds and serve as conduits for the release of terrestrially derived GHG. Low-gradient streams contain pool structures with longer residence times conducive to the in-situ production of GHG, but these streams, and the longitudinal heterogeneity therein, are seldom studied. We measured continuous ecosystem metabolism alongside concentrations and fluxes of carbon dioxide (CO_2), methane (CH_4) and nitrous oxide (N_2O) from autumn to the following spring along an eight kilometer segment of a low-gradient third order stream in the North Carolina Piedmont. We characterized spatial and temporal patterns of GHG in the context of channel geomorphology, hydrology, and ecosystem metabolic rates using linear mixed effects models. We found that stream metabolic cycling was responsible for most of the CO_2 flux over this period, and that in-channel aerobic metabolism was a primary driver of both CH_4 and N_2O fluxes as well. Long water residence times, limited reaeration, and substantial organic matter from terrestrial inputs foster conditions conducive to the in-stream accumulation of CO_2 and CH_4 from microbial respiration. Streams like this one are common in landscapes with low topographic relief, making it likely that the high contribution of instream metabolism to GHG fluxes that we observed is a widespread yet understudied behavior of many small streams.

Plain Language Summary (optional):

Stream ecosystems play a role in producing greenhouse gases and transporting them from groundwater to be released into the atmosphere. Some of these gases are produced through the breakdown of organic matter by microbes in the stream. We don't know how important this microbial production is compared to gases coming from soil and groundwater, but comparing it to rates of ecosystem metabolism may help us learn about it. We measured greenhouse gas and metabolism along a stream and found that metabolism is directly responsible for the production of carbon dioxide and is a good predictor of methane, meaning that microbial production in the stream is likely important. Nitrous oxide production was limited by competition between microbes for nitrogen, as a result, the stream was removing nitrous oxide from the atmosphere rather than releasing it.

1 Introduction

A large fraction of the carbon fixed in terrestrial ecosystems is exported to streams as dissolved carbon dioxide (CO_2) and methane (CH_4), dissolved organic matter, and particulate organic matter. In most rivers these terrestrial carbon subsidies exceed the inputs of carbon from aquatic photosynthesis (Webster & Meyer, 1997), and are the dominant source of energy fueling aquatic ecosystem metabolism (Roberts et al., 2007). Rivers represent important landscape control points (sensu Bernhardt et al., 2017) by both efficiently transporting and degassing terrestrially derived CO_2 and CH_4 (GHG_{terr}) and by actively mineralizing terrestrial organic matter and respiring it as CO_2 and CH_4 (GHG_{aq}) (Hotchkiss et al., 2015). We increasingly recognize that gaseous C emissions from freshwater ecosystems are an important component of regional and global carbon cycles that considerably offset estimates of terrestrial carbon sequestration (Battin et al., 2009; J. Cole et al., 2007; Holgerson & Raymond, 2016), that

greenhouse gas emissions from streams represent a significant contribution to atmospheric forcing (Quick et al., 2019; Raymond et al., 2013), and that small headwater streams are important locations for GHG release in river networks (Li et al., 2021; Stanley et al., 2016).

Despite their importance for global forcing, estimates of GHG concentrations and fluxes in streams are still poorly constrained, in part due to high spatial and temporal variability. Many physical (Crawford et al., 2013; Lupon et al., 2019) and chemical (Schade et al., 2016) drivers have been shown to underly this variability, while studies that incorporate ecosystem metabolic cycling as a driver are less common (Crawford et al., 2014). It has been widely assumed that aquatic production of greenhouse gases is likely to be important only in large rivers (J. J. Cole & Caraco, 2001; Hotchkiss et al., 2015; Vannote et al., 1980), but recent studies have shown that mineralization of organic matter can be a primary source of river GHG fluxes in some headwater streams as well (Rocher-Ros et al., 2020). In aquatic ecosytems photosynthesis and aerobic respiration directly control oxygen concentrations and thus may indirectly regulate the production of methane and nitrous oxide (N_2O) via anaerobic respiratory pathways (Megonigal et al., 2004). Positive relationships between aerobic respiration and methane fluxes have been observed (Stanley et al., 2016), and may arise due either to a shared dependence on organic carbon substrates or to the indirect control of redox conditions by respiring aerobes. Nitrous oxide production in rivers has received far less attention, but tends to be quite low, even for polluted rivers where rates of nitrification and denitrification are high (Beaulieu et al., 2011).

Climate change is altering the timing, magnitude and spatial distribution of both terrestrial GHG delivery and aquatic GHG production in rivers. Changes in groundwater recharge are expected as a result of changing precipitation patterns and higher evapotranspiration in terrestrial ecosystems (Taylor et al., 2013). Decreased groundwater delivery at baseflow will

likely reduce the magnitude of emissions derived from terrestrial sources, and increase the importance of riverine metabolism in driving GHG fluxes. In contrast, for rivers where climate change leads to flashier hydrology, riverine metabolic processes may be constrained by disturbance (Bernhardt et al., 2022), enhancing the relative importance of terrestrially derived GHGs (Blackburn & Stanley, 2021) and likely enhancing interannual variability in GHG concentrations and fluxes (Junker et al., 2020). In all rivers, warming temperatures may drive higher rates of in stream carbon processing (Yvon-Durocher et al., 2010) and the production of CO_2 and CH_4 (Demars et al., 2016; Yvon-Durocher et al., 2014), pushing the carbon balance in streams toward faster mineralization reduced storage and transport.

We measured oxygen and greenhouse gas concentrations along an eight kilometer segment of New Hope Creek in the North Carolina Piedmont. This site is a heterotrophic, low-gradient stream with a forested catchment. Rates of instream gross primary productivity (GPP) are highest from late winter until the canopy closes in April, while rates of ecosystem respiration (ER) peak following litterfall in October (Carter, 2021; C. A. S. Hall, 1972). To capture both periods of peak instream metabolic activity our study extended from the end of autumn through the productivity peak in the following spring. Over the course of these three seasons, we measured dissolved oxygen concentrations continuously and calculated daily rates of stream GPP and ER at six sites for each date on which we collected gas concentration and gas flux measurements. We examined the relationship between gas dynamics and physical and biogeochemical drivers using linear mixed effects models and gas ratios. Our goals were to: 1) characterize the patterns and magnitudes of greenhouse gas concentrations and fluxes, 2) determine potential drivers of gas dynamics, and 3) describe the role of in stream processing in generating and consuming GHGs in New Hope Creek through space and time.

2 Methods

2.1 Site Description

The New Hope Creek watershed is located in the North Carolina Piedmont within Durham and Orange Counties, NC at 36 N, -79 E. In the 8.5 km stream section in this study, New Hope Creek is a 3rd order stream and flows through a fully forested section of the Duke Forest (Figure 1). The study watershed (delineated to the outlet of our study reach, see below) is 81 km^2 with 90% forest cover, 9% agricultural land and 1.3% developed land based on 2016 NLCD data (Carter, 2021). The study reach has an average depth of 0.4 m and width of 14.4 m measured in March and an average slope of 3.2 m/km. Along this section, New Hope Creek is in the Triassic basin and the stream alternates between long deep pools and short bedrock outcrops that create riffles (see Figure S1 for photos). Even during periods of steady flow, there is no measurable water velocity in the large pools and water residence times last from hours up to several days. Seasonally, discharge varies several orders of magnitude between high flow storm peaks throughout the winter and spring, and frequent, extended dry periods in autumn. This study was initiated when flow resumed, after a period of no flow in October when the creek had become a series of disconnected pools. During our study from November 2019 - March 2020 there was constant stream flow with a median of 0.7 m3/s at the outlet.

Our six monitoring sites spanned an 8.5 km reach starting at the most upstream site at 0 km (NHC_0) to the outlet of our reach at the downstream point NHC_8.5. All sites are named based on their distance in km from the top to the bottom of the reach. Two of the sites are in long deep pools: NHC_2.3 (2330 m), and NHC_6.9 (6880m). Three sites are in shorter pools that often transitioned to runs: NHC_0 (0 m), NHC_5 (5000 m), and NHC_8.5 (8450 m). One site is in a run downstream of a riffle: NHC_2.5 (2500 m), Figure 1. We measured the distance to each

of these sites starting at 8.5 km and walking up the stream channel with a hip chain (Forestry Supply) counting distance in meters. We measured the latitude and longitude of each site using a handheld GPS and paired them with reaches in the National Hydrography Dataset (NHD) (USGS, 2019) using the nhdplusTools package (Blodgett, 2019) in R (R core team, v. 3.6.3) to obtain the contributing watershed area for each site.

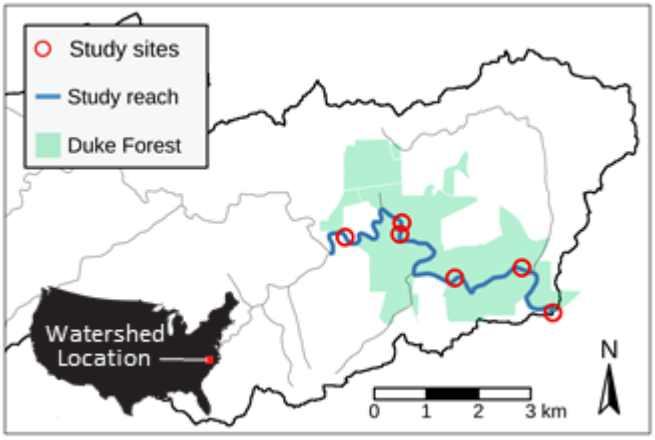

Figure 1. Map of the New Hope Creek watershed with study sites labeled as red points. The study reach spans 8.5 km and is contained entirely within the Duke Forest (in green).

2.2 Sensor deployment

At each of our monitoring locations, we collected continuous measurements of dissolved oxygen concentrations and temperature (Onset HOBO U26, Bourne, MA, USA), and water pressure (Onset HOBO U20L) at 15-minute intervals from November 2019 - March 2020. We deployed sensors attached to a fence post at all sites except for NHC_8.5, which was mounted directly to bedrock, in the thalweg of the stream or one meter from the side of the stream in deep pool sites (NHC_7, and NHC_2.3). The sensors were mounted inside of a 3” PVC pipe with many 1” holes drilled to allow for complete water flow. These PVC cages were placed so that the

sensors were measuring at ~25 cm below the surface during average baseflow. We calibrated the dissolved oxygen sensors in the lab prior to deployment by placing them in 100% air saturated water as the 100% saturation point. To do this, bubbled a bucket of water with ~20 L of room temperature water with air forced through a ceramic aquaculture stone for one hour then allowed the bucket to equilibrate for 10 minutes to avoid measuring supersaturated water. For a 0% saturation point, we placed the sensors in a 1M sodium sulfite solution until they equilibrated. We deployed dissolved oxygen sensors with copper antibiofouling caps. During the deployment period, we visited the sensors at least biweekly to clear debris and clean biofilms from the sensor and PVC housing with a brush and to download data.

2.3 Hydrology and Channel Morphology

We modeled discharge at the upstream (NHC_0) and downstream (NHC_8.5) monitoring sites based on continuous water level data collected by pressure transducers. Over a range of flow conditions, we measured stream discharge by velocity profiling with an electromagnetic sensor (Marsh-McBirney Flo-Mate, Frederick, MD, USA) and built site specific level-discharge rating curves based on measurements at NHC_0 (n = 11) and NHC_8.5 (n = 13) with a bank-full high flow point added at each site by calculating flow based on Manning's equation for open channel flow. To estimate discharge at the intervening sites, we assumed that flow accumulation was proportional to accumulated upslope area (Leach et al., 2017) during periods when the stream was gaining flow and that flow loss was proportional to stream length during periods of losing flow and calculated discharge by interpolating the continuous measurements from sites NHC_0 and NHC_8.5. Flow did not exceed the maximum points on our discharge rating curves for any of our GHG sampling dates.

194 We conducted channel morphology surveys in the 1km reaches upstream of NHC_0 and
195 NHC_8.5 by measuring cross-sections of depth, channel width, and stream bank heights every
196 100 m for a total of 10 locations at each site. We followed the streamPULSE geomorphic survey
197 protocol (streampulse.org) to collect these measurements. From these 20 cross sections, we
198 developed a linear relationship between thalweg depth and average channel depth. We conducted
199 two separate surveys of the entire 8.5 km study reach measuring channel width and thalweg
200 depth every 50 m at high flow (9 Mar 2019) and at low flow (8 Oct 2019). We converted thalweg
201 depths to average depth according to our empirical relationship and used this data to calculate
202 average depth in the 1 km reach above each sensor site at two separate time points (Carter,
203 2021). We paired these depth measurements with discharge estimates calculated for each site on
204 the respective days and used this pair of points to calculate site specific parameters for this
205 empirical depth (D) by discharge (Q) relationship (Leopold & Maddock, 1953):

206 $$D = cQ^f \qquad \textit{(eq 1)}$$

207

208 where c is the average depth at unit discharge and f is a unitless coefficient.

209 At each sensor location, we calculated stream bed slope from a 30 m resolution LiDAR
210 map of the study watershed available through the North Carolina State University Libraries
211 (https://www.lib.ncsu.edu/gis/elevation). We used the continuous_stream_slope function in the
212 whiteboxTools package (Lindsay, 2014) in R (v 3.6.3) to extract stream slopes from the LiDAR
213 images.

214

215 2.4 Water Chemistry analyses

216 We measured dissolved ions, dissolved organic carbon, and dissolved gas concentrations

on eleven different dates from 11 Nov 2019 - 21 Mar 2020 at intervals ranging from 1-3 weeks. At each sample date, we collected a water sample for laboratory analyses from all six monitoring locations. We measured water temperature, conductivity, pH, and dissolved oxygen and atmospheric pressure at the time of sample collection with a handheld meter (Yellow Springs Instruments, Columbus, OH, USA). We collected water from ~ 15 cm below the surface and filtered it through ashed 25 mm GF/F filters into acid washed HDPE 60 ml bottles. We kept water samples on ice until they could be frozen at -20 C until analysis. We analyzed the water samples for nitrate (NO_3-N) on a Dionex ion chromatograph (ICS-2000) with a KOH eluent generator and an IonPac AS-18 analytical column (Dionex Corporation, Sunnyvale, CA, USA). The minimum detection limit (mdl) for NO_3^- was 5 μg N/L. We measured ammonium (NH_4^+-N, phenate method, mdl = 5 μg N/L) and soluble reactive phosphorus (SRP, ascorbic acid method, mdl = 2.5 μg/L) on a Lachat QuikChem 8000 (Lachat Instruments, Milwaukee, WI, USA). We analyzed total dissolved nitrogen (TDN, mdl = 0.05 mg/L) and dissolved organic carbon (DOC, mdl = 0.25 mg/L) on a Shimadzu TOC-V total carbon analyzer that had a TNM-1 nitrogen module (Shimadzu Scientific Instruments, Colombia, MD, USA). We set concentrations that were below detection to one half of the minimum detection limits.

2.5 Dissolved Gas

We collected dissolved gas samples in duplicate alongside each water sample and used laboratory headspace equilibration to obtain a gas sample for analysis (adapted from Hudson, 2004). We used pre-weighed, 60-ml crimp-capped glass serum vials that were evacuated in the laboratory no more than 24 hrs in advance of sampling. In the field, we collected a water sample by placing the evacuated vial 5-10 cm below the surface of the water, inserting a 20 gauge needle

and allowing the vial to fill to ~40 ml before removing the needle below the water surface. On multiple sample days, we also collected atmospheric samples in evacuated 9 ml glass serum vials at the sample sites. We kept samples on ice until returning to the laboratory where we immediately equilibrated them. We determined the volume of each sample by weight with a Mettler Toledo PB precision balance (0.01 g). To equilibrate samples, we added N_2 gas with a glass syringe to the evacuated headspace until vials were at atmospheric pressure, then added an additional 15 ml of N_2. We then placed the vials on a shaker table for two minutes to allow the dissolved gases to equilibrate with the nitrogen headspace. After shaking, we transferred 10 ml of headspace from each sample into an evacuated 9-ml glass serum vial using a glass syringe. We then immediately uncapped the samples and measured water temperature and lab air pressure for equilibration calculations. On the day of equilibration, we prepared a 5 point standard curve in triplicate in evacuated 9 ml serum vials that we stored with the samples until analysis, always within two weeks of sample collection.

We analyzed gas samples for carbon dioxide (CO_2), methane (CH_4) and nitrous oxide (N_2O) in the extracted headspace within two weeks of collection. We conducted our analyses with a Shimadzu 17A gas chromatograph equipped with an electron capture detector (ECD) and a flame ionization detector (FID, Shimadzu Scientific Instruments, Colombia, MD). To allow for determination of multiple gas concentration from the same sample, we attached sixport valves and a methanizer. Duplicate samples were injected with a Tekmar 7050 Headspace Autosampler and run with ultra-high purity N2 as the carrier gas and a P5 mixture as the make-up gas for the ECD. Medical grade breathing air was plumbed through a Nafion tube to remove water vapor from the sample stream. We used a five point standard curve of known concentrations (certified primary standards, Airgas, Morrisville, NC, USA) to convert peak areas of samples into gas

concentrations.

We calculated the dissolved gas concentration in the water sample based on the headspace concentration (see below for analysis) following Hudson 2004. First we calculated the aqueous concentration of the gas that was partitioned into the headspace during equilibration (C_{AH}).

$$C_{AH} = \frac{V_h}{V_w} \times C_g \times \rho_g \quad \textit{(eq 2)}$$

Where V_h is the volume of N_2 in the headspace and V_w is the volume of water, C_g is the measured gas concentration in ml/ml and ρ_g is the density of the gas (mg/L). We then calculated the concentration of gas still in the aqueous phase after equilibration (C_A) using gas specific Henry's Law constants (H, atm/mol fraction):

$$C_A = \frac{p_g}{H} \times \frac{n_w}{V_w} \times MW_g \quad \textit{(eq 3)}$$

Where p_g is the partial pressure of the gas at lab atmospheric pressure, n_w/V_w is the molar concentration of water (55.5 mol/L) and MW_g is the molecular weight of the gas (mg/L). The total concentration of gas in the water sample (C, mg/L) is:

$$C = C_{AH} + C_A \quad \textit{(eq 4)}$$

2.6 Gas Flux

We estimated gas fluxes to the atmosphere (F, mg/m2/d) for each sample using:

$$F = (C - C_{sat}) \times k_g \quad \textit{(eq 5)}$$

where C (mg/L) is the dissolved gas concentration in the water, C_{sat} (mg/L) is the saturation concentration of the gas at equilibrium with the atmosphere (calculated using Henry's law), and k_g (m d^{-1}) is the gas exchange coefficient for a specific gas (Raymond et al., 2012). The geomorphology in New Hope Creek is dominated by long deep pools where average water velocities are low, even during moderate flow when water volume is high (~0.1 m/s at 1 m^3/s) resulting in low gas exchange velocities and long turnover distances for dissolved gases (3v/k ~ 5 km, (Chapra & Di Toro, 1991). Because of this, open channel methods for measuring gas exchange with a tracer gas (R. O. Hall & Madinger, 2018) do not produce reliable results. We therefore estimated gas exchange coefficients using inverse modeling based on dissolved oxygen time series (R. O. Hall & Ulseth, 2020) calculating k for each day based on the pooled relationship between K_{600} and discharge at each site (Appling et al., 2018; Figure S2, see Metabolism section for details). We converted our model derived estimates of k_{600} (m d^{-1}), which is the gas exchange coefficient normalized to a Schmidt number of 600, to gas specific values (k_g, m d^{-1}) according to:

$$k_g = \left(\frac{Sc_g}{600}\right)^{(-1/2)} / k_{600} \qquad \textit{(eq 6)}$$

Using the gas specific schmidt numbers (Sc_g) calculated at the sample water temperature according to the coefficients in Raymond 2012.

We used the calculated K values for each gas along with average velocity (v) to estimate the turnover 95% length of the gas as ~3v/K (Chapra & Di Toro, 1991). These estimates were almost always greater than our 1 km "footprints" upstream of each sensor site.

2.7 Metabolism

We modeled metabolism based on the single station diel O_2 method using the hierarchical bayesian state space model StreamMetabolizer (Appling, Hall, Arroita, et al., 2018) in R (v. 3.6.3). This model estimates daily rates of gross primary productivity (GPP), ecosystem respiration (ER) and the gas exchange coefficient K600 based on changes in oxygen concentration over time according to:

$$\frac{dO_2}{dt} = GPP_t + ER_t + k_{O_2} \times (DO_i - DO_{sat,i}) \quad \textit{(eq 7)}$$

Where kO_2 (m d^{-1}) is the oxygen specific gas exchange coefficient related to K600 by the schmidt number for O_2 (Eq 6), DO_i and $DO_{sat,i}$ are the instantaneous concentration of dissolved oxygen and the concentration at saturation in the stream, and GPP_t, ER_t are daily, volumetric rates (g $O_2/m^3/d$). We used a model with both observation and process error and with partial pooling of K600, which restricts the amount of variation allowed in the K600 by discharge relationship to reduce equifinality in model solutions (Appling, Hall, Yackulic, et al., 2018). We ran the model with uninformative priors on GPP and ER and with a weak prior on K600 with a mean calculated based on empirical relationships for headwater streams (Raymond et al., 2012) and a standard deviation of 0.7 at each node in the K-Q relationship (for more details on model fitting of our data, see Carter 2021). After estimating metabolism, we removed model estimates for which the R_{hat}, a metric of parameter convergence, was above 1.05 or for which ER was greater than zero or GPP less than zero with a 95% CI that did not contain zero.

329 2.8 Data Analysis

330 To determine how gas concentrations and fluxes varied along with hypothesized physical
331 and biological drivers we fit the following models:

332 $$y_{i,j} = \boldsymbol{\beta X_{i,j}} + u_i + v_j + \varepsilon_{i,j} \quad \textit{(eq 8)}$$

333 $$u_{\boldsymbol{i}} \sim N(0, \sigma^2_{meas})$$

334 $$v_{\boldsymbol{j}} \sim N(0, \sigma^2_{site})$$

335 $$\varepsilon_{\boldsymbol{i,j}} \sim N(0, \sigma^2_{proc})$$

336 where $y_{i,j}$ is the gas concentration or flux for the i^{th} sample at the j^{th} site, $\boldsymbol{\beta}$ is a vector of
337 coefficients, $\mathbf{X}_{i,j}$ is a vector of measured covariates $(1, x_1, \ldots, x_n)_{i,j}$ for each sample and site.
338 Residual variation is partitioned into measurement error (variation between replicates: u_i), and
339 process error which includes unexplained variation between sites (v_j) and unexplained residual
340 variation ($\varepsilon_{i,j}$). We performed model selection in R (v 4.1.3, R Core Team, 2022) with the lme4
341 package (Bates et al., 2015) using the code: lmer(y ~ (1|rep) + (1|site) + x1 + … + xn) on z-
342 scored data and predictors. Each baseline model contained a random intercept for sample
343 replicate, subsequent models added a random intercept for site and different combinations of
344 stream geomorphic characteristics (stream slope and average depth), physical properties (water
345 temperature and discharge), stream metabolism (GPP, ER), and water chemistry (concentration
346 of NO_3^-, DOC, O_2).

347 We conducted model selection based on Akaike's Information Criterion corrected for
348 small sample sizes (AIC_c, Hurvich & Tsai, 1989) and restricted possible models to those that
349 contained 5 or fewer fixed effects and did not allow inclusion of both discharge and dissolved
350 organic carbon, which are highly correlated ($r = 0.82$, $p < 0.001$). All other predictors have $r <$
351 0.6, but to prevent multicollinearity, we only considered models with variance inflation factors

(VIF) of less than 5 (Beier et al., 2001). Nitrate was only included in models for N_2O concentration and flux. Average depth was included in models for gas concentrations but not fluxes as depth was used directly in the calculations of gas flux. We present the top five models for each gas in supplementary table S1 and the single best models in tables 1 and 2. For the best fit models, we calculated a marginal R^2, which describes the variance explained by just the fixed effects ($x_1, \ldots, x_n$) and a conditional R^2, which is the variance explaned by the whole model including random intercepts (Nakagawa & Schielzeth, 2013).

To further evaluate the links between greenhouse gases and stream metabolism, we calculated the fraction of O_2 and CO_2 flux that could be explained by aerobic metabolism by first calculating the rate of gas production or consumption due to net ecosystem metabolism (NEP = GPP - ER). We converted oxygen based metabolism estimates to units of CO_2 using a respiratory quotient (RQ) of 0.8 measured as moles of CO_2 produced per mole of O_2 consumed. We used the reciprocal of this (1.25) as a photosynthetic quotient (PQ). We calculated the fraction of instream contribution as NEP_g/F_g (the gas specific NEP rate divided by the gas flux rate). If this fraction was larger than one, we considered that to be 100% contribution. If this fraction was negative (ie gas flux to the atmosphere and gas consumption by NEP) we considered that to be 0% contribution.

For oxygen, carbon dioxide and methane, we calculated the gas departure from atmospheric equilibrium for each sample. This is the amount of dissolved gas in excess of the saturation concentration, or the saturation deficit if the gas is undersaturated. We calculated gas specific saturation concentrations based on temperature and the atmospheric partial pressure using Henry's Law. The gas departure represents a source (e.g. groundwater, production) or a sink (e.g. consumption, oxidation) of the gas other than exchange with the atmosphere (Vachon

et al., 2020). We present the molar ratios of CO_2:O_2 departures and CH_4:CO_2 departures and discuss various biogeochemical processes in the context of these ratios.

3 Results

3.1 Gas concentrations and fluxes

We measured dissolved gas concentrations at six sites on dates spanning November to March for a total of 58 site by date combinations. The concentration of oxygen (O_2) ranged from 6.9 to 12.4 mg/L (mean ± std. dev: 10.5 ± 1.1 mg/L), carbon dioxide (CO_2) ranged from 0.2 to 7.1 mg/L (2.3 ± 1.4 mg/L), methane (CH_4) ranged from 0.7 to 20.5 μg/L (4.3 ± 3.4 μg/L), and nitrous oxide (N_2O) ranged from 0 to 0.86 μg/L (0.48 ± 0.21 μg/L). On average, oxygen was undersaturated and was dissolving from the atmosphere (-1.8 ± 1.7 $g/m^2/d$). The stream was nearly always effluxing CO_2 (2.9 ± 2.5 $g/m^2/d$) and CH_4 (6.9 ± 4.7 $mg/m^2/d$), while N_2O switched from undersaturated to supersaturated during the study with fluxes ranging from -1.4 to 0.71 $mg/m^2/d$ (-0.22 ± 0.52 $mg/m^2/d$, Figure 2). While there were some consistent patterns of increasing or decreasing concentrations between sites, when averaged across all sample dates only CH_4 concentration was significantly different across sites ($F = 5.2$, $p = 0.0006$). Gas fluxes did not differ significantly across sites for any gas (Figure 2).

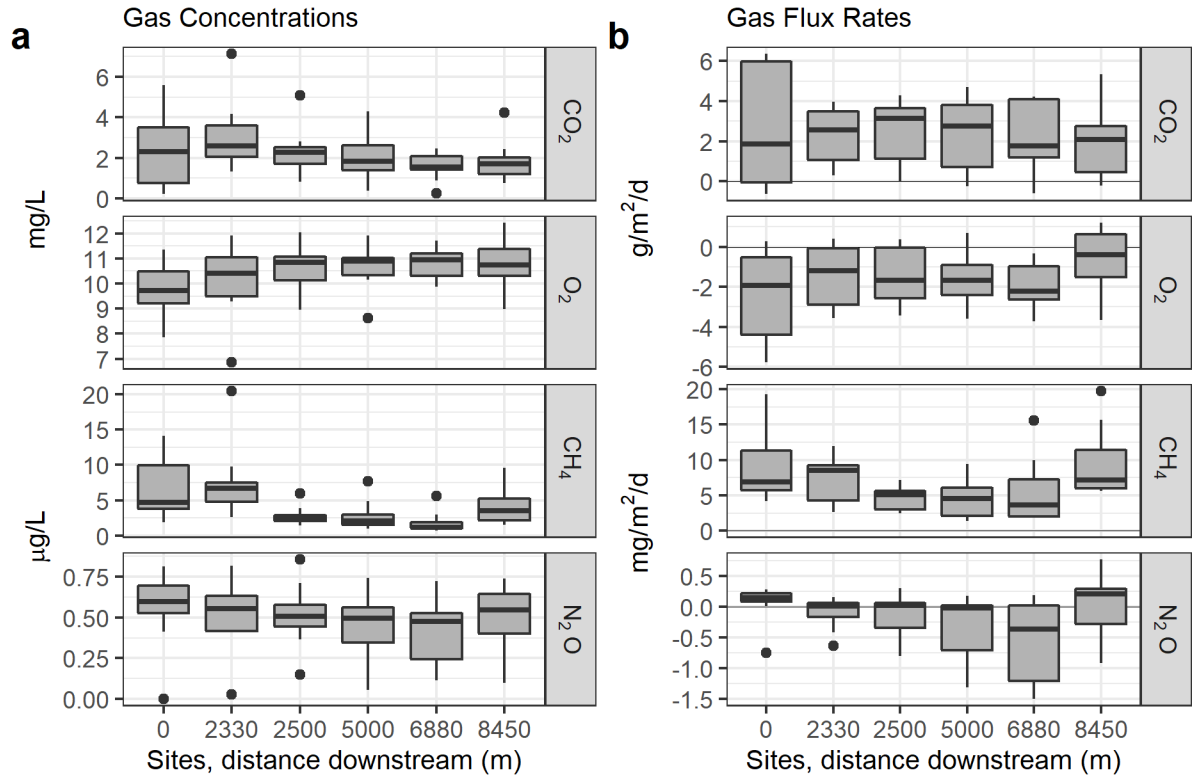

Figure 2. Longitudinal variation in dissolved gas (a) concentrations and (b) fluxes at each of the six study sites. Box plots show the distributions across all sample dates (n = 11).

There was more variation in gas concentrations and fluxes over time than over space (Figure 3). From November to March, each dissolved gas showed a different pattern. Dissolved oxygen was low in November, (8.8 ± 1.4 mg/L) and increased throughout the winter, peaking in late January (11.8 ± 0.4 mg/L). Carbon dioxide started at its highest point in November (5.2 ± 1.2 mg/L) and decreased through March to a minimum of 0.6 ± 0.4 mg/L. Methane also had its peak in November (11 ± 6.4 μg/L) then decreased to a winter mean of 2.9 ± 1.8 μg/L before rising in the spring to 7.5 ± 2 μg/L by the end of March. Nitrous oxide did not have consistent temporal trends; concentration was at its minimum in mid-November (0.07 ± 0.06 μg/L), its maximum in late January (0.78 ± 0.05 μg/L) and is the most variable in early December (0.41 ± 0.27 μg/L) (Figure 3). Gas fluxes out of the stream show similar patterns to their concentrations

404 with the exception that N_2O switches from being absorbed by the stream from November to mid-
405 January to degassing from the stream for the remainder of the spring.
406

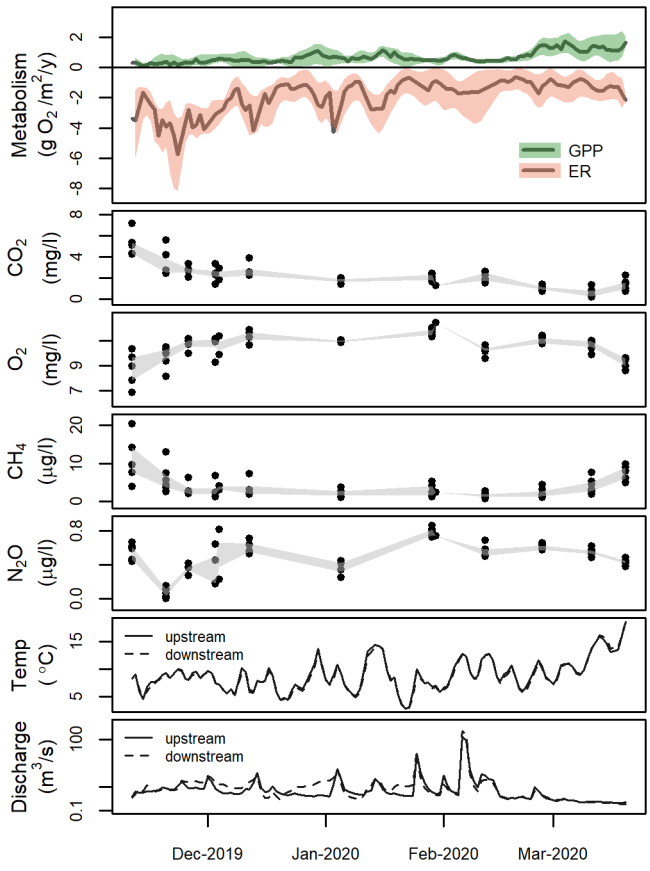

Figure 3. High temporal variation in gas concentrations and predictors from 11-Nov-2019 to 21-Mar-2020 across all six sampling sites in New Hope Creek. From top to bottom: mean daily gross primary productivity (GPP) and ecosystem respiration (ER) shown with 95% CIs; gas concentrations with samples from all sites shown as points and the interquartile range shaded grey; mean daily water temperature and discharge (Q) at the upstream (0 m) and downstream (8450 m) sites.

407

408 Best fit linear mixed effects models explained 80, 76, and 49% of the variation in CO_2,
409 CH_4, and N_2O concentrations and 66, 55, and 46% of the variation in fluxes respectively based
410 on variation in fixed effects. Variation across sites helped predict CO_2 concentration with
411 unmeasured site characteristics explaining ~6% of unmodeled variability as a random effect. For
412 CH_4 concentration and flux, the slope of stream sites was a better predictor than site alone, with
413 steeper stream beds predicting less CH_4. Stream discharge varied by over an order of magnitude

between sampling dates (Figure 4) with higher flows predicting higher CO_2 fluxes but lower CH_4 and N_2O concentrations. Because of the strong positive correlation between discharge and dissolved organic carbon (DOC), we consider the relavance of both predictors when one was selected, suggesting that N_2O fluxes may also decrease with higher flows.

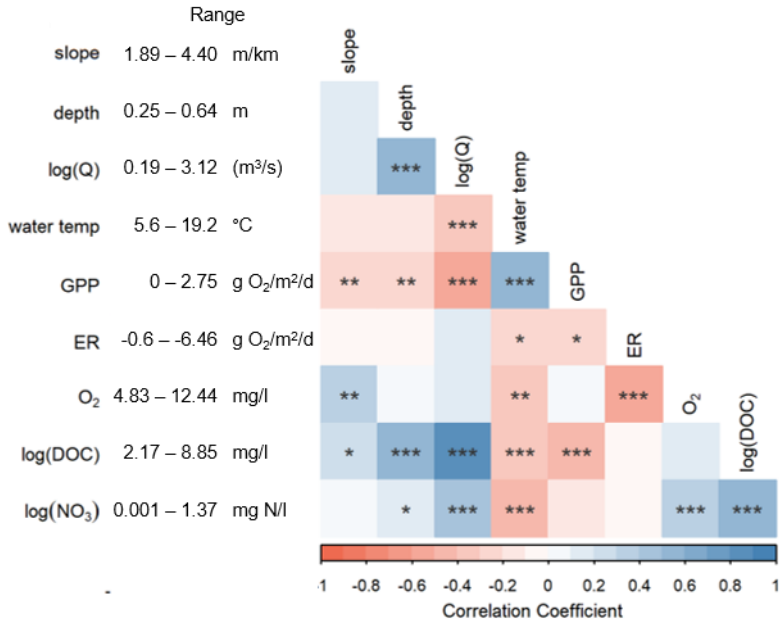

Figure 4. Correlations and ranges of predictor variables. Ranges are for values on sampling dates before log scaling. Significant relationships at $p \leq 0.01$, 0.05, and 0.1 are indicated by ***, **, and * respectively.

Stream metabolism was selected as a predictor in every model (Table 1). More primary productivity (GPP) predicted lower concentrations and fluxes of CO_2 and CH_4. More respiration (ER) predicted lower concentration and flux of N_2O. While ER wasn't selected as a predictor for CO_2 or CH_4, less oxygen, which is correlated with higher ER (Figure 4), predicts more of both gases. Interestingly, N_2O flux is negatively predicted by both ER and O_2, despite their negative covariance, suggesting that they reflected independent controls. Finally, variation in water chemistry significantly predicts N_2O with more nitrate predicting higher concentrations and fluxes and more DOC predicting lower N_2O. Considering discharge as a proxy for DOC, may suggest that higher DOC is linked to higher CO_2 and lower CH_4. Across all models,

428 measurement error (σ^2_{meas}) accounted for ~15% (0.15 sdev) of the unmodeled variability in CO_2,

429 18% (0.27 sdev) in CH_4, and 29% (0.38 sdev) in N_2O (Table 2).

430

Table 1. Best models for each gas concentration and flux.

Model		**w_{AICc}**	**R^2 m**	**R^2 c**	**VIF**	**Model Predictors**
CO_2	conc	59%	0.797	0.980	1.98	Site + Temp + GPP + O_2
	flux	48%	0.661	0.970	1.60	log(Q) + GPP + O_2
CH_4	conc	45%	0.757	0.948	1.66	Slope + log(Q) + GPP + O_2
	flux	60%	0.553	0.871	1.64	Slope + Temp + GPP + ER
N_2O	conc	38%	0.489	0.866	1.24	log(Q) + ER + log(NO_3)
	flux	46%	0.463	0.850	1.65	ER + O_2 + log(DOC) + log(NO_3)

All models include a random intercept for sample replicate in addition to the listed predictors. Best model was selected based on AICc (see table S1). w_{AICc}: Model weight out of top 5 models, R^2m: Marginal R^2 (fit of fixed effects), R^2c: Conditional R^2 (fit including random effects), VIF: variance inflation factor. See text for details.

431

Table 2. Model estimates and uncertainties for each of the top models

Model		**Slope**	**Q**†	**Temp**	**ER**	**GPP**	**O_2**	**DOC**†	**NO_3**†	**σ^2_{site}**	**σ^2_{proc}**	**σ^2_{meas}**
CO_2	conc	–	–	-0.55**	–	-0.21*	-0.81**	–	–	0.056	0.127	0.020
	flux	–	0.59**	–	–	-0.23*	-0.44**	–	–		0.311	0.030
CH_4	conc	-0.36**	-0.45**	–	–	-0.32**	-0.54**	–	–		0.193	0.053
	flux	-0.42**	–	0.40**	0.45**	-0.57**	–	–	–		0.329	0.134
N_2O	conc	–	-0.42**	–	-0.35**	–	–	–	0.59**		0.386	0.137
	flux	–	–	–	-0.67**	–	-0.49**	-0.37**	0.53**		0.400	0.155

Model estimates are given for each selected predictor with * and ** indicating significance at the 0.01 and 0.001 levels respectively. Standard deviations of random intercepts are shown for between sites (σ^2_{site}), between replicates (σ^2_{meas}) and residual unexplained variation attributed to process error (σ^2_{proc}). All values are based on z-scored data. †Discharge (Q), dissolved organic carbon (DOC), and nitrate (NO_3) are all on a log scale.

3.2 Gas Dynamics and Metabolism

In stream production of carbon dioxide by aerobic respiration (ER) contributed substantially to the total flux of carbon dioxide. We calculated rates of CO_2 production from net ecosystem production (NEP) assuming a respiration quotient (RQ) of 0.8 (but see SI for an exploration or RQ ranging from 0.6 - 1). In-stream NEP was negative on 117 of 131 days, and for clarity we refer to this excess of respiration over photosynthetic assimilation as net heterotrophy (sensu Hall, 1972). Net heterotrophy accounted for 64% of the total CO_2 efflux from the stream across all sampling dates and locations. Across sampling days, the net heterotrophic contribution to CO_2 efflux spanned the full range from 0% (NEP $\geq$ 0, or CO_2 flux $\leq$ 0) to 100% (Net heterotrophy $\geq$ CO_2 flux). In autumn, when litter inputs and high temperatures

443 stimulated high rates of ER and there was limited groundwater inflow, net heterotrophy
444 accounted for 78 ± 20% of the CO_2 flux. In the spring, when fluxes of photosynthesis were
445 highest and sometimes exceeding fluxes of ER, net heterotrophy accounted for only 27 ± 40% of
446 the CO_2 flux. We measured the lowest net contribution of heterotrophy to total CO_2 fluxes in our
447 late February sampling (17 ± 40%), which took place on the falling limb of a large storm (Figure
448 5).
449

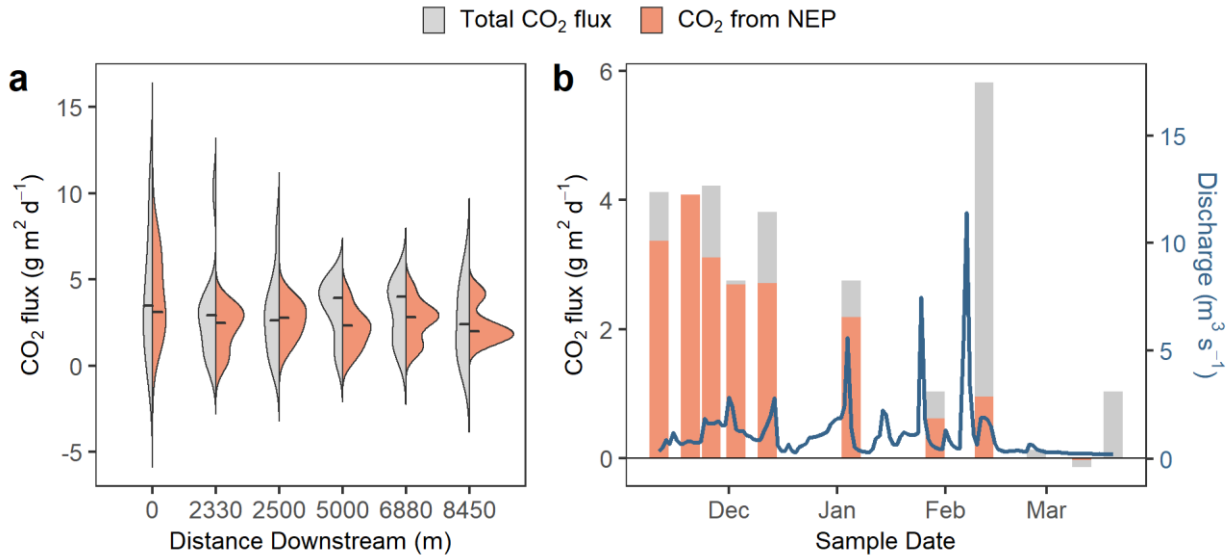

Figure 5. Almost all of the CO_2 flux is accounted for by in stream metabolism except on the falling limb of a large storm. (a) Grey distributions on the left show the range of CO_2 fluxes across all dates which had positive flux at each site and orange distributions on the right show CO_2 generated by net ecosystem productivity (NEP) for those same days with a respiration quotient (RQ) of 0.8. Distribution medians are indicated by horizontal lines. (b) Bars show total CO_2 flux across sites on each sample date with the fraction attributable to NEP colored orange. Discharge at the outlet of the reach is shown on a linear scale in blue.

450

451 The role of aerobic metabolism in shaping gas dynamics is reflected in the relationship
452 between the molar departures of O_2 and CO_2 from atmospheric equilibrium (Figure 5a).
453 Atmospheric exchange will tend to push both gases toward zero departure from equilibrium, and
454 gas concentrations varying only as a result of gross primary productivity and aerobic metabolism
455 would result in a negative relationship passing through the origin (Vachon et al., 2020). Across
456 our samples, CO_2 and O_2 departures were negatively correlated (Figure 5a) and span a gradient
457 from high O_2 and low CO_2 when the stream was autotrophic (NEP ~ 0.5 g $O_2/m^2/d$) to low O_2
458 and high CO_2 when the stream was heterotrophic (NEP ~ -6 g $O_2/m^2/d$).The slope is a 1:1 line of
459 oxygen depletion and carbon dioxide production which is higher than a typical respiratory
460 quotient (RQ, moles CO_2 produced per mole O_2 consumed) for heterotrophic systems. We show
461 the literature based RQ of 0.8 (del Giorgio & Peters, 1994) that we used to calculate the above
462 contributions of NEP to CO_2 flux in Figure 5. Indeed, if we calculate the moles of CO_2
463 consumed by NEP as the slope of a regression line between NEP and the CO_2 departure
464 ($dCO_2/dNEP$, $r^2 = 0.431$, $p < 0.0001$) and divide this by the similarly derived $dO_2/dNEP$ ($r^2 =$
465 0.623, $p < 0.0001$), we arrive at a respiratory quotient of 0.76, supporting this assumption. Both
466 the flatter slope of this line and the positive intercept suggest there are additional inputs of CO_2
467 from other sources.
468

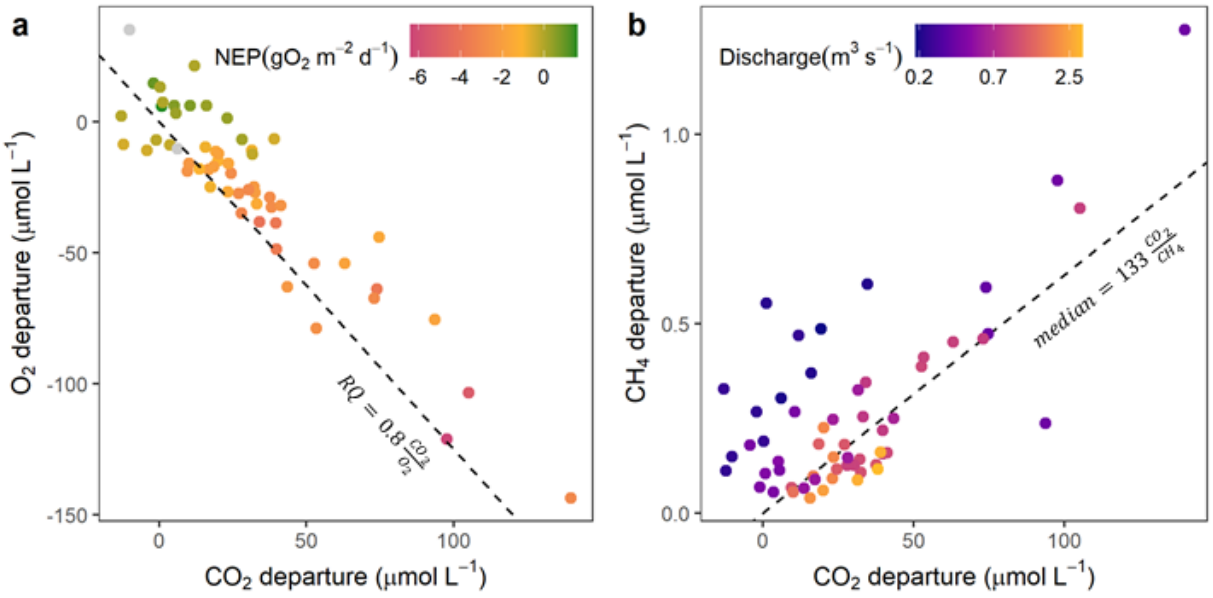

Figure 6. Gas ratios suggest instream controls. (A) Dissolved CO_2 and O_2 in excess of the stream water saturation value for each gas sample. The line represents the pattern that would be expected in diel data corresponding with a respiratory quotient of 0.8 moles CO_2 produced per mole O_2. The points are colored by net ecosystem productivity (GPP + ER).
(B) Dissolved CH_4 in excess of stream saturation plotted against excess CO_2.The data have a wide spread around a median molar ratio of 133 with purple indicating that samples with low discharge tend to be enriched in CH_4 while yellow points show high discharge samples which are CH_4 depleted relative to CO_2.

469

470 Methane concentrations covaried with carbon dioxide concentration with an average
471 molar departure ratio of 0.0031 ± 0.15. The variance around this relationship is much higher than
472 it is for O_2 and CO_2 and much of the spread around the line is related to stream discharge (Figure
473 5b). In general, samples taken at low discharge were enriched in CH_4 relative to CO_2 while those
474 taken at high discharge were depleted. Much of this variation is seasonal; autumn and winter
475 CH_4:CO_2 ratios average ~ 0.005 with the lowest in early November and in the spring they

increase to ~0.12 with a few exceptionally high values. This increase overlaps with the spring productivity bloom and associated CO_2 depletion which drives at least part of the shift. However, CH_4 concentrations also increase in the spring, contributing to the shift. Nitrous oxide departures from saturation do not covary with any of the other gases.

4 Discussion

Over the course of this 9 month study, New Hope Creek was a net source of carbon dioxide and methane to the atmosphere and a net sink of nitrous oxide. Aerobic metabolism within the stream channel was the dominant driver of carbon dioxide dynamics and was likely important for methane and nitrous oxide as well. Seasonal variation in stream metabolism and hydrology drives most of the observed patterns. During late autumn, respiration derived from the pulse of terrestrial litterfall was high, driving oxygen depletion, nitrate limitation, and carbon dioxide supersaturation. In the spring, algal photosynthesis led to a period of oxygen supersaturation and carbon dioxide depletion. Methane concentrations followed similar seasonal patterns as carbon dioxide with even larger magnitude shifts. Throughout the fall respiration peak, nitrous oxide concentrations were well below saturation, but both nitrate and nitrous oxide concentrations increased in spring as the system moved towards autotrophy. This may indicate that nitrous oxide production was limited by nitrate, depleted by heterotrophic bacteria in the fall. We suggest that the high predictability of GHG concentrations and fluxes by instream controls is a result of low hyporheic and atmospheric exchange, a claim supported by the low channel complexity, flat stream gradients, and frequent long deep pools in New Hope Creek.

4.1 Magnitudes and Patterns

Carbon dioxide (CO_2) concentrations in New Hope Creek are comparable to those observed in similarly sized streams, but flux rates are much lower due to limited gas exchange. A synthesis of US streams reports an average CO_2 concentration of 5.3 mg/L and flux of 18.9 g $CO_2/m^2/d$ in 3rd order streams (Butman & Raymond, 2011). While the total flux from New Hope Creek is lower, the fraction of carbon dioxide flux due to in stream metabolism is comparable to that in some streams (Rocher-Ros et al., 2020) but higher than is reported in most streams of similar size (Gómez-Gener et al., 2016; Lupon et al., 2019; Rasilo et al., 2017). The fraction we measured is likely a conservative estimate, as we would expect the lowest contribution of instream metabolism during the winter, which is when we collected most of our measurements. Methane (CH_4) concentrations and fluxes are an order of magnitude lower than is on the global average concentration reported in a recent synthesis (22 +-83 μg/L) but are about equal to that of other undisturbed reference streams (~5 μg/L, Stanley et al., 2016). Nitrous oxide (N_2O) concentrations vary substantially across streams and rivers, and our concentrations are lower than most. This might be because many N_2O studies are done in places where nitrate is high such as urban streams and agricultural streams, with average N_2O about three times as high as in NHC (1.2 μg/L, Beaulieu et al., 2008). A synthesis from Quick et al 2019 reports nitrous oxide fluxes ranging from -3 up to several thousand $mg/m^2/d$. While most studies in this synthesis show streams as a net source of N_2O to the atmosphere, some, particularly in forested areas, report very low concentrations and occasional net absorption of N_2O (e.g., -2 to 6 $mg/m^2/d$, Soued et al., 2016).

4.2 Metabolism controls

Instream aquatic metabolism was a dominant control on gas concentrations and fluxes in New Hope Creek during this study. Photosynthesis and aerobic respiration are directly responsible for the consumption and production of carbon dioxide and explain a large fraction of variation in gas concentrations. In the autumn, mineralization of terrestrial leaf litter by stream heterotrophs is responsible for almost all the CO_2 flux to the atmosphere. At times, net heterotrophic respiratory production of CO_2 is much higher than the CO_2 flux to the atmosphere, leading to an accumulation of CO_2 in the stream, even when it is already supersaturated. This has been reported in arctic streams (Rocher-Ros et al., 2020), but has not previously been reported for low order streams like New Hope Creek which have previously been shown to derive the bulk of their CO_2 flux to the atmosphere from groundwater inputs (Duvert et al., 2019; Hotchkiss et al., 2015; Rasilo et al., 2017). In part, this accumulation is due to a limited ability to exchange with the atmosphere. New Hope Creek is deep and slow moving, even in the winter months, and dissolved gas often remains in the water column for several days and in transit over multiple kilometers due to limited gas exchange. This can cause lags between gas production and degassing and creates ideal conditions for oxygen depletion driving the system hypoxic during periods of low flows and high temperatures (Carter et al., 2021).

While our metabolic rates do not incorporate measurements of anaerobic processes, they nonetheless serve as a strong predictor of methane concentration and flux. The “anaerobic scaling hypothesis” suggests that anaerobic respiration may scale with aerobic respiration, allowing CO_2 or ER to serve as a predictor for methane concentrations (Stanley et al., 2016). This relationship can arise via two distinct but not mutually exclusive mechanisms. First, aerobic respiration depletes oxygen, so periods of high aerobic respiration can lead to oxygen depletion

which favors anaerobic methanogenesis while low respiration may sustain high oxygenconcentrations which can facilitate methane oxidation in the water column (Stanley et al., 2016). An alternative mechanisms is that both aerobic respiration and methane production are stimulated whenever there are large allochthonous organic matter subsidies such as terrestrial litterfall (Roberts et al., 2007) or DOC pulses from storm flows (Demars, 2019).

Even when the stream water column is well oxygenated, measurable methane concentrations and fluxes are present, indicating the potential for respiration at all levels on the redox ladder to be co-occurring throughout the sediments. When respiration increases, so does the CH_4:CO_2 ratio, meaning that the fraction of respiration occuring through CH_4 producing pathways is increasing. This might indicate that electron acceptors are more limiting than organic carbon in anoxic microsites and CH_4 production proceeds in the absence of more energetically favorable electron acceptors (Megonigal et al., 2004). Indeed, the sediments contain large amounts of buried organic carbon, and storms frequently replenish dissolved organic carbon in the water column (Zimmer & McGlynn, 2018).

In New Hope Creek, the anaerobic scaling hypothesis did not extend to nitrous oxide, an intermediate product of both anaerobic (denitrification) and aerobic (nitrification) metabolic pathways (Quick et al., 2019). Some studies have found that increased respiration predicts nitrous oxide fluxes from streams (Beaulieu et al., 2011; Madinger & Hall, 2019; Reisinger et al., 2016). This relationship may arise when high organic matter availability drives both aerobic respiration and denitrification, or if respiratory demand depletes oxygen, favoring the use of nitrate as an alternative electron acceptor to fuel anaerobic respiration via denitrification (Rosamond et al., 2012). In New Hope Creek, we do see a slight increase in N_2O fluxes with lower oxygen, but this relationship is not strong. Instead, in New Hope Creek, fluxes of N_2O

566 between the stream and atmospere shift from outgassing when respiration is low to net influx at
567 times of high respiration. In fact, the stream was a net sink of N_2O during the autumn respiration
568 peak at the same time that it was acting as a large source of both CH_4 and CO_2.

569 Throughout the autumn, nitrate appears to be limiting N_2O production as denitrifiers are
570 out-competed by aerobic heterotrophs during the respiration peak. In the winter and spring,
571 nitrate demand drops in the absence of large terrestrial organic matter subsidies and N_2O
572 concentrations and fluxes slowly catch up and remain high through the spring. Nitrogen is not
573 limiting in the spring in New Hope Creek (Covino et al., 2018), and denitrifiers are able to
574 coexist with autotrophs. Additionally, the response of CH_4 production to increased respiration is
575 not as strong in the spring as in the autumn. One possible explanation of this is that methane
576 production is reduced in by greater availability of NO_3, which is a more energetically favorable
577 electron acceptor than organic carbon (Megonigal et al., 2004).

578 4.3 Physical controls

579 In stream physical drivers are also important in predicting gas dynamics. Concentrations
580 of CO_2 were consistently lower during periods of warmer water temperatures. This result is
581 somewhat counterintutive given the well documented increases in metabolic rates with
582 temperature (Yvon-Durocher et al., 2012; Zhu et al., 2020), but can be explained because the
583 high energy input to the stream via litterfall occurs during the late autumn when temperatures are
584 colder (Bernhardt et al., 2022; Demars et al., 2016). Though substrate supply overrides any affect
585 of temperature on metabolic CO_2 production, warmer temperatures do reduce the solubility of
586 GHG, contributing to enhanced degassing. In combination reduced solubility and reduced
587 substrate supply lead to lower CO_2 concentrations in warmer months.

588 Long water residence times may favor anaerobic metabolism (Gomez-Gener et al., 2020).
589 We see a distinct shift toward higher CH_4:CO_2 ratios with lower discharge in New Hope Creek.
590 An increase in anaerobic processes with low discharge may be attributed to higher groundwater
591 exchange or porewater seepage (Taillardat et al., 2022), the development of anoxic regions
592 within the channel, or less atmospheric exchange. Geomorphologies that have consistently low
593 water velocities such as pools tend to accumulate fine sediments that settle out of the water
594 column, creating conditions conducive to sediment hypoxia (Stanley et al., 2016). All these
595 factors suggest there would be a greater accumulation of metabolic byproducts at low discharge,
596 and it is likely that with longer residence times, a greater proportion of those byproducts will be
597 from lower on the redox ladder.

598 Storm flows shift the controls on gas flux away from instream production in favor of
599 terrestrial inputs. The only sampling date where less than half of the CO_2 flux was derived from
600 instream production was on the falling limb of a large storm. This could be explained by large
601 amounts of terrestrial CO_2 entering in from groundwater during the storm (Jones & Mulholland,
602 1998), or by the opportunistic venting of a large quantity of CO_2 that had accumulated in the
603 stream, trapped by low gas exchange. This suggests that while instream controls dominate in
604 New Hope Creek on average, storms may serve as temporal control points when infrequent but
605 large inputs of inorganic carbon control the budget.

606

607 4.4 Spatial controls

608 Although most of the variation in gases in New Hope Creek was seasonal, we did observe
609 consistent spatial patterns across sampling dates. This variation appears to be related to channel
610 structure, with flatter segments with longer water residence times characterized by lower oxygen

concentrations and the accumulation of more respiration byproducts. Methane is more linked to local variability than the other gases, and there were consistent control points where methane concentrations were higher, suggesting production from anaerobic metabolism or input from groundwater. The spatial variability in all gases was the highest in the autumn respiration peak; a low flow time when the stream was likely to be losing water (Zimmer & McGlynn, 2017) which would result in minimal groundwater inputs and less mixing with the hyporheic zone (Fox et al., 2014), conditions which favor anaerobic metabolic pathways.

In New Hope Creek, small, often steep, bedrock riffles separate the large pools and create points of turbulent mixing, even at low flows. They serve as control points for gas evasion, especially in this low gradient stream where gas exchange coefficients are universally low elsewhere. These exert strong control on gas evasion and consistently move gases toward equilibrium with the atmosphere in all seasons (Rocher-Ros et al., 2019).

5 Conclusions

Trace gas fluxes out of New Hope Creek are low relative to ranges reported in the literature (Quick et al., 2019; Raymond et al., 2013; Stanley et al., 2016). Long water residence times, low groundwater inputs and limited reaeration create ideal conditions for instream metabolic processes to drive GHG concentrations and fluxes. At times, instream photosynthesis is high enough to deplete stream CO_2 below saturation and during periods of peak heterotrophic respiration the river becomes a net sink for N_2O. It is this seasonal variation in instream GPP and ER that drives the temporal variation in GHGs observed throughout New Hope Creek. We also see consistent differences between river segments linked to channel geomorphology. River segments with the longest water residence times store substantial quantities of organic matter and

634 are primary sources of respiratory products (Casas-Ruiz et al., 2017; Gómez-Gener et al., 2015),
635 while rare high velocity sections act as the control points at which the majority of GHGs are
636 vented to the atmosphere (Rocher-Ros et al., 2019). Our results suggest that organic matter
637 inputs and storage along with nutrient limitation determine the timing and magnitude of gas
638 production while hydrologic regimes and hydraulic gradients constrain these rates and determine
639 the balance between instream controls and external sources. Climate change is altering all these
640 drivers of riverine GHG production and flux, and we anticipate the combination of lower gas
641 solubility and more frequent hypoxia will lead to higher CO_2 and CH_4 fluxes and may shift New
642 Hope Creek from a sink to a source of N_2O. Since the geomorphic conditions and human
643 modifications that lead to high organic matter and water residence times in New Hope Creek are
644 not unique (Wohl & Merritts, 2007), we suspect that similar trends will be observed in low
645 gradient headwater streams throughout the world.
646

647 **Acknowledgments**

648 This research was done on the ancestral lands of the Haliwa-Saponi, Sappony, and Occaneechi-
649 Saponi nations. We thank Brooke Hassett, Alexander Miele, Cathy Chamberlin, Johnny Behrens,
650 Wyatt Jernigan, and Emily Ury for asstance with field and laboratory work; and Ashley Helton,
651 Bob Hall, Jim Heffernan, and Martin Doyle for conceptual development and helpful comments
652 on a draft of this manuscript. Funding for this work was from NSF Macrosystems award number
653 1442439 and EPSCoR award number 2019528.
654

655 **Open Research Statement**

656 The greenhouse gas data and all covariates used for this manuscript and the code used to
657 complete all analyses and generate the figures are available at zenodo via DOI
658 10.5281/zenodo.6977566 with a GPL 3.0 license.
659

660 ## References

661 Appling, A. P., Hall, R. O., Yackulic, C. B., & Arroita, M. (2018). Overcoming Equifinality: Leveraging Long Time
662 Series for Stream Metabolism Estimation. *Journal of Geophysical Research: Biogeosciences*, *123*(2), 624–
663 645. https://doi.org/10.1002/2017JG004140

664 Appling, A. P., Hall, R. O., Arroita, M., & Yackulic, C. B. (2018). streamMetabolizer: Models for Estimating
665 Aquatic Photosynthesis and Respiration. R package. (Version 0.10.9). Retrieved from
666 https://github.com/USGS-R/streamMetabolizer

667 Bates, D., Mächler, M., Bolker, B. M., & Walker, S. C. (2015). Fitting linear mixed-effects models using lme4.
668 *Journal of Statistical Software*, *67*(1). https://doi.org/10.18637/jss.v067.i01

669 Battin, T. J., Luyssaert, S., Kaplan, L. A., Aufdenkampe, A. K., Richter, A., & Tranvik, L. J. (2009). The boundless
670 carbon cycle. *Nature Geoscience*, *2*(9), 598–600. https://doi.org/10.1038/ngeo618

671 Beaulieu, J. J., Arango, C. P., Hamilton, S. K., & Tank, J. L. (2008). The production and emission of nitrous oxide
672 from headwater streams in the Midwestern United States. *Global Change Biology*, *14*(4), 878–894.
673 https://doi.org/10.1111/j.1365-2486.2007.01485.x

674 Beaulieu, J. J., Tank, J. L., Hamilton, S. K., Wollheim, W. M., Hall, R. O., Mulholland, P. J., et al. (2011). Nitrous
675 oxide emission from denitrification in stream and river networks. *Proceedings of the National Academy of*
676 *Sciences of the United States of America*, *108*(1), 214–219. https://doi.org/10.1073/pnas.1011464108

677 Beier, P., Burnham, K. P., & Anderson, D. R. (2001). *Model Selection and Inference: A Practical Information-*
678 *Theoretic Approach*. *The Journal of Wildlife Management* (Vol. 65). https://doi.org/10.2307/3803117

679 Bernhardt, E. S., Blaszczak, J. R., Ficken, C. D., Fork, M. L., Kaiser, K. E., & Seybold, E. C. (2017). Control Points
680 in Ecosystems: Moving Beyond the Hot Spot Hot Moment Concept. *Ecosystems*, *20*(4), 665–682.
681 https://doi.org/10.1007/s10021-016-0103-y

682 Bernhardt, E. S., Savoy, P., Vlah, M. J., Appling, A. P., Koenig, L. E., Jr, R. O. H., et al. (2022). Light and flow
683 regimes regulate the metabolism of rivers. *Proceedings of the National Academy of Sciences*, *119*(8), 5.
684 https://doi.org/10.1073/pnas.2121976119
685 Blackburn, S. R., & Stanley, E. H. (2021). Floods increase carbon dioxide and methane fluxes in agricultural
686 streams. *Freshwater Biology*, *66*(1), 62–77. https://doi.org/10.1111/fwb.13614
687 Blodgett, D. (2019). nhdplusTools: Tools for Accessing and Working with the NHDPlus, version 0.3.8,
688 https://code.usgs.gov/water/nhdplusTools.
689 Butman, D., & Raymond, P. A. (2011). Significant efflux of carbon dioxide from streams and rivers in the United
690 States. *Nature Geoscience*, *4*(12), 839–842. https://doi.org/10.1038/ngeo1294
691 Carter, A. M. (2021). *Shifting thermal and metabolic regimes in a low gradient, temperate river network*
692 (Dissertation). Duke University. Retrieved from https://hdl.handle.net/10161/23088
693 Carter, A. M., Blaszczak, J. R., Heffernan, J. B., & Bernhardt, E. S. (2021). Hypoxia dynamics and spatial
694 distribution in a low gradient river. *Limnology & Oceanography*, *66*(6), 2251–2265.
695 https://doi.org/10.1002/lno.11751
696 Casas-Ruiz, J. P., Catalán, N., Gómez-Gener, L., von Schiller, D., Obrador, B., Kothawala, D. N., et al. (2017). A
697 tale of pipes and reactors: Controls on the in-stream dynamics of dissolved organic matter in rivers.
698 *Limnology and Oceanography*, *62*, S85–S94. https://doi.org/10.1002/lno.10471
699 Chapra, S. C., & Di Toro, D. M. (1991). Delta Method for Estimating Primary Production, Respiration, and
700 Reaeration in Streams. *Journal of Environmental Engineering*, *117*(5), 640–655.
701 Cole, J., Prairie, Y. T., Caraco, N. F., McDowell, W. H., Tranvik, L. J., Striegl, R. G., et al. (2007). Plumbing the
702 global carbon cycle: Integrating inland waters into the terrestrial carbon budget. *Ecosystems*, *10*(1), 171–
703 184. https://doi.org/10.1007/s10021-006-9013-8
704 Cole, J. J., & Caraco, N. F. (2001). Carbon in catchments: Connecting terrestrial carbon losses with aquatic
705 metabolism. *Marine and Freshwater Research*, *52*(1), 101–110. https://doi.org/10.1071/MF00084
706 Covino, T. P., Bernhardt, E. S., & Heffernan, J. B. (2018). Measuring and interpreting relationships between nutrient
707 supply, demand, and limitation. *Freshwater Science*, *37*(3), 448–455. https://doi.org/10.1086/699202

708 Crawford, J. T., Striegl, R. G., Wickland, K. P., Dornblaser, M. M., & Stanley, E. H. (2013). Emissions of carbon
709 dioxide and methane from a headwater stream network of interior Alaska. *Journal of Geophysical*
710 *Research: Biogeosciences*, *118*(2), 482–494. https://doi.org/10.1002/jgrg.20034
711 Crawford, J. T., Lottig, N. R., Stanley, E. H., Walker, J. F., Hanson, P. C., Finlay, J. C., et al. (2014). CO2 and CH4
712 emissions from streams in a lake-rich landscape: Patterns, controls, and regional significance. *Global*
713 *Biogeochemical Cycles*, *28*, 197–210. https://doi.org/10.1002/2013GB004661
714 Demars, B. O. L. (2019). Hydrological pulses and burning of dissolved organic carbon by stream respiration.
715 *Limnology and Oceanography*, *64*(1), 406–421. https://doi.org/10.1002/lno.11048
716 Demars, B. O. L., Gíslason, G. M., Ólafsson, J. S., Manson, J. R., Friberg, N., Hood, J. M., et al. (2016). Impact of
717 warming on CO2 emissions from streams countered by aquatic photosynthesis. *Nature Geoscience*, *9*(10),
718 758–761. https://doi.org/10.1038/ngeo2807
719 Duvert, C., Bossa, M., Tyler, K. J., Wynn, J. G., Munksgaard, N. C., Bird, M. I., et al. (2019). Groundwater-Derived
720 DIC and Carbonate Buffering Enhance Fluvial CO2 Evasion in Two Australian Tropical Rivers. *Journal of*
721 *Geophysical Research: Biogeosciences*, *124*(2), 312–327. https://doi.org/10.1029/2018JG004912
722 Fox, A., Boano, F., & Arnon, S. (2014). Impact of losing and gaining streamflow conditions on hyporheic exchange
723 fluxes induced by dune-shaped bed forms. *Water Resources Research*, *50*(3), 1895–1907.
724 https://doi.org/10.1002/2013WR014668
725 del Giorgio, P. A., & Peters, R. H. (1994). Patterns in planktonic P:R ratios in lakes: Influence of lake trophy and
726 dissolved organic carbon. *Limnology and Oceanography*, *39*(4), 772–787.
727 https://doi.org/10.4319/lo.1994.39.4.0772
728 Gómez-Gener, L., Obrador, B., von Schiller, D., Marcé, R., Casas-Ruiz, J. P., Proia, L., et al. (2015). Hot spots for
729 carbon emissions from Mediterranean fluvial networks during summer drought. *Biogeochemistry*, *125*(3),
730 409–426. https://doi.org/10.1007/s10533-015-0139-7
731 Gómez-Gener, L., von Schiller, D., Marcé, R., Arroita, M., Casas-Ruiz, J. P., Staehr, P. A., et al. (2016). Low
732 contribution of internal metabolism to carbon dioxide emissions along lotic and lentic environments of a
733 Mediterranean fluvial network. *Journal of Geophysical Research: Biogeosciences*, *121*(12), 3030–3044.
734 https://doi.org/10.1002/2016JG003549

735 Gomez-Gener, L., Lupon, A., Laudon, H., & Sponseller, R. A. (2020). Drought alters the biogeochemistry of boreal
736 stream networks. *Nature Communications*, *11*(1795). https://doi.org/10.1038/s41467-020-15496-2
737 Hall, C. A. S. (1972). Migration and Metabolism in a Temperate Stream Ecosystem. *Ecology*, *53*(4), 585–604.
738 Hall, R. O., & Madinger, H. L. (2018). Use of argon to measure gas exchange in turbulent mountain streams.
739 *Biogeosciences*, *15*(10), 3085–3092. https://doi.org/10.5194/bg-15-3085-2018
740 Hall, R. O., & Ulseth, A. J. (2020). Gas exchange in streams and rivers. *WIREs Water*, *7*(1), 1–18.
741 https://doi.org/10.1002/wat2.1391
742 Holgerson, M. A., & Raymond, P. A. (2016). Large contribution to inland water CO2and CH4emissions from very
743 small ponds. *Nature Geoscience*, *9*(3), 222–226. https://doi.org/10.1038/ngeo2654
744 Hotchkiss, E. R., Hall Jr, R. O., Sponseller, R. A., Butman, D., Klaminder, J., Laudon, H., et al. (2015). Sources of
745 and processes controlling CO2 emissions change with the size of streams and rivers. *Nature Geoscience*,
746 *8*(9), 696–699. https://doi.org/10.1038/ngeo2507
747 Hudson, F. (2004). Sample Preparation and Calculations for Dissolved Gas Analysis in Water Samples Using a GC
748 Headspace Equilibration Technique. *British Journal of Dermatology*, *151*(2), 1–14.
749 https://doi.org/10.1111/j.1365-2133.2004.v151_is68_disclaimer.x
750 Hurvich, C. M., & Tsai, C. L. (1989). Regression and time series model selection in small samples. *Biometrika*,
751 *76*(2), 297–307. https://doi.org/10.1093/biomet/76.2.297
752 Jones, J. B., & Mulholland, P. J. (1998). Influence of drainage basin topography and elevation on carbon dioxide
753 and methane supersaturation of stream water. *Biogeochemistry*, *40*(1), 57–72.
754 https://doi.org/10.1023/A:1005914121280
755 Junker, J. R., Cross, W. F., Benstead, J. P., Huryn, A. D., Hood, J. M., Nelson, D., et al. (2020). Flow is more
756 Important than Temperature in Driving Patterns of Organic Matter Storage and Stoichiometry in Stream
757 Ecosystems. *Ecosystems*. https://doi.org/10.1007/s10021-020-00585-6
758 Leach, J. A., Lidberg, W., Kuglerová, L., Peralta-Tapia, A., Ågren, A., & Laudon, H. (2017). Evaluating
759 topography-based predictions of shallow lateral groundwater discharge zones for a boreal lake-stream
760 system. *Water Resources Research*, *53*(7), 5420–5437. https://doi.org/10.1002/2016WR019804
761 Leopold, L. B., & Maddock, T. (1953). The Hydraulic Geometry of Stream Channels and Some Physiographic
762 Implications. *USGS Professional Paper*, (252).

763 Li, M., Peng, C., Zhang, K., Xu, L., Wang, J., Yang, Y., et al. (2021). Headwater stream ecosystem: an important
764 source of greenhouse gases to the atmosphere. *Water Research*, *190*.
765 https://doi.org/10.1016/j.watres.2020.116738
766 Lindsay, J. B. (2014). The Whitebox Geospatial Analysis Tools project and open-access GIS. In *Proceedings of the*
767 *GIS research UK 22nd Annual Conference*. The University of Glasgow, 16-18 April.
768 https://doi.org/10.13140/RG.2.1.1010.8962
769 Lupon, A., Denfeld, B. A., Laudon, H., Leach, J., Karlsson, J., & Sponseller, R. A. (2019). Groundwater inflows
770 control patterns and sources of greenhouse gas emissions from streams. *Limnology and Oceanography*,
771 *64*(4), 1545–1557. https://doi.org/10.1002/lno.11134
772 Madinger, H. L., & Hall, R. O. (2019). Linking denitrification with ecosystem respiration in mountain streams.
773 *Limnology and Oceanography Letters*, *4*(5), 145–154. https://doi.org/10.1002/lol2.10111
774 Megonigal, J. P., Hines, M. E., & Visscher, P. T. (2004). Anaerobic Metabolism: Linkages to Trace Gases and
775 Aerobic Processes. In W. H. Schlesinger (Ed.), *Biogeochemistry* (pp. 317–424). Elsevier Pergamon,
776 Oxford, UK. https://doi.org/10.1016/B0-08-043751-6/08132-9
777 Nakagawa, S., & Schielzeth, H. (2013). A general and simple method for obtaining R2 from generalized linear
778 mixed-effects models. *Methods in Ecology and Evolution*, *4*(2), 133–142. https://doi.org/10.1111/j.2041-
779 210x.2012.00261.x
780 Quick, A. M., Benner, S. G., Reeder, W. J., Farrell, T. B., Tonina, D., & Feris, K. P. (2019). Nitrous oxide from
781 streams and rivers : A review of primary biogeochemical pathways and environmental variables. *Earth-*
782 *Science Reviews*, *191*(March 2018), 224–262. https://doi.org/10.1016/j.earscirev.2019.02.021
783 R Core Team. (2022). R: A language and environment for Statistical Computing. Vienna, Austria: R Foundation for
784 Statistical Computing. Retrieved from https://www.R-project.org/
785 Rasilo, T., Hutchins, R. H. S., Ruiz-González, C., & del Giorgio, P. A. (2017). Transport and transformation of soil-
786 derived CO2, CH4 and DOC sustain CO2 supersaturation in small boreal streams. *Science of The Total*
787 *Environment*, *579*, 902–912. https://doi.org/10.1016/j.scitotenv.2016.10.187
788 Raymond, P. A., Zappa, C. J., Butman, D., Bott, T. L., Potter, J., Mulholland, P., et al. (2012). Scaling the gas
789 transfer velocity and hydraulic geometry in streams and small rivers. *Limnology and Oceanography: Fluids*
790 *and Environments*, *2*(1), 41–53. https://doi.org/10.1215/21573689-1597669

Raymond, P. A., Hartmann, J., Lauerwald, R., Sobek, S., McDonald, C., Hoover, M., et al. (2013). Global carbon dioxide emissions from inland waters. *Nature*, *503*(7476), 355–359. https://doi.org/10.1038/nature12760

Reisinger, A. J., Tank, J. L., Hoellein, T. J., & Hall, R. O. (2016). Sediment, water column, and open-channel denitrification in rivers measured using membrane-inlet mass spectrometry. *Journal of Geophysical Research: Biogeosciences*, *121*, 1258–1274. https://doi.org/10.1002/2015JG003261.Received

Roberts, B. J., Mulholland, P. J., & Hill, W. R. (2007). Multiple scales of temporal variability in ecosystem metabolism rates: Results from 2 years of continuous monitoring in a forested headwater stream. *Ecosystems*, *10*(4), 588–606. https://doi.org/10.1007/s10021-007-9059-2

Rocher-Ros, G., Sponseller, R. A., Lidberg, W., Mörth, C., & Giesler, R. (2019). Landscape process domains drive patterns of CO2 evasion from river networks. *Limnology and Oceanography Letters*, 87–95. https://doi.org/10.1002/lol2.10108

Rocher-Ros, G., Sponseller, R. A., Bergström, A. K., Myrstener, M., & Giesler, R. (2020). Stream metabolism controls diel patterns and evasion of CO2 in Arctic streams. *Global Change Biology*, *26*(3), 1400–1413. https://doi.org/10.1111/gcb.14895

Rosamond, M. S., Thuss, S. J., & Schiff, S. L. (2012). Dependence of riverine nitrous oxide emissions on dissolved oxygen levels. *Nature Geoscience*, *5*(10), 715–718. https://doi.org/10.1038/ngeo1556

Schade, J. D., Bailio, J., & McDowell, W. H. (2016). Greenhouse gas flux from headwater streams in New Hampshire, USA: Patterns and drivers. *Limnology and Oceanography*, *61*, S165–S174. https://doi.org/10.1002/lno.10337

Soued, C., Giorgio, P. A., & Maranger, R. (2016). Nitrous oxide sinks and emissions in boreal aquatic networks in Québec, *9*, 116–120. https://doi.org/10.1038/NGEO2611

Stanley, E. H., Casson, N. J., Christel, S. T., Crawford, J. T., Loken, L. C., & Oliver, S. K. (2016). The ecology of methane in streams and rivers: patterns, controls, and global significance. *Ecological Monographs*, *86*(2), 146–171.

Taillardat, P., Bodmer, P., Deblois, C. P., Ponçot, A., Prijac, A., Riahi, K., et al. (2022). Carbon Dioxide and Methane Dynamics in a Peatland Headwater Stream: Origins, Processes and Implications. *Journal of Geophysical Research: Biogeosciences*, *127*(7), e2022JG006855. https://doi.org/10.1029/2022JG006855

Taylor, R. G., Scanlon, B., Döll, P., Rodell, M., van Beek, R., Wada, Y., et al. (2013). Ground water and climate change. *Nature Climate Change*, *3*(4), 322–329. https://doi.org/10.1038/nclimate1744

USGS. (2019). National Hydrography Dataset (ver. USGS National Hydrography Dataset Plus High Resolution for Hydrologic Unit 2 - 03), accessed June 23, 2020.

Vachon, D., Sadro, S., Bogard, M. J., Lapierre, J., Baulch, H. M., Rusak, J. A., et al. (2020). Paired O2 –CO2 measurements provide emergent insights into aquatic ecosystem function. *Limnology and Oceanography Letters*, *5*(4), 287–294. https://doi.org/10.1002/lol2.10135

Vannote, R. L., Minshall, W. G., Cummins, K. W., Sedell, J. R., & Cushing, C. E. (1980). The River Continuum Concept. *Canadian Journal of Fisheries and Aquatic Science*, *37*, 130–137.

Webster, J. R., & Meyer, J. L. (1997). Organic Matter Budgets for Streams: A Synthesis. *Journal of the North American Benthological Society*, *16*(1), 141–161. https://doi.org/10.2307/1468247

Wohl, E., & Merritts, D. J. (2007). What Is a Natural River? *Geography Compass*, *1*(4), 871–900. https://doi.org/10.1111/j.1749-8198.2007.00049.x

Yvon-Durocher, G., Jones, J. I., Trimmer, M., Woodward, G., & Montoya, J. M. (2010). Warming alters the metabolic balance of ecosystems. *Philosophical Transactions of the Royal Society B: Biological Sciences*, *365*(1549), 2117–2126. https://doi.org/10.1098/rstb.2010.0038

Yvon-Durocher, G., Caffrey, J. M., Cescatti, A., Dossena, M., Giorgio, P. Del, Gasol, J. M., et al. (2012). Reconciling the temperature dependence of respiration across timescales and ecosystem types. *Nature*, *487*(7408), 472–476. https://doi.org/10.1038/nature11205

Yvon-Durocher, G., Allen, A. P., Bastviken, D., Conrad, R., Gudasz, C., St-Pierre, A., et al. (2014). Methane fluxes show consistent temperature dependence across microbial to ecosystem scales. *Nature*, *507*(7493), 488–491. https://doi.org/10.1038/nature13164

Zhu, Y., Purdy, K. J., Eyice, Ö., Shen, L., Harpenslager, S. F., Yvon-Durocher, G., et al. (2020). Disproportionate increase in freshwater methane emissions induced by experimental warming. *Nature Climate Change*, *10*(7), 685–690. https://doi.org/10.1038/s41558-020-0824-y

Zimmer, M. A., & McGlynn, B. L. (2017). Bidirectional stream–groundwater flow in response to ephemeral and intermittent streamflow and groundwater seasonality. *Hydrological Processes*, *31*(22), 3871–3880. https://doi.org/10.1002/hyp.11301

Zimmer, M. A., & McGlynn, B. L. (2018). Lateral, Vertical, and Longitudinal Source Area Connectivity Drive Runoff and Carbon Export Across Watershed Scales. *Water Resources Research*, *54*(3), 1576–1598. https://doi.org/10.1002/2017WR021718